*Korean J. Chem. Eng.*, 38(2), 454-460 (2021)
DOI: 10.1007/s11814-020-0695-y

pISSN: 0256-1115
eISSN: 1975-7220

# Composite solid polymer electrolyte with silica filler for structural supercapacitor applications

**Minsik Hwang‡, Ji San Jeong‡, Jae-Chul Lee, Seongil Yu, Hyun Seok Jung, Bong-Sang Cho, and Ki-Young Kim†**

Human Convergence Technology R&D Department, Research Institute of Convergence Technology, Korea Institute of Industrial Technology (KITECH), Gyeonggi-do 15588, Korea
(*Received 19 May 2020 • Revised 24 September 2020 • Accepted 14 October 2020*)

**Abstract**−Structural supercapacitors are energy storage devices that can function as structural materials. We synthesized composite solid polymer electrolytes (CSPEs) from 1-ethyl-3-methylimidazolium trifluoromethanesulfonate ([EMIm][OTF]), poly (ethylene glycol) monomethyl ether acrylate (PEGA) and functionalized silica filler. Two types of fumed silica were used: one had an unmodified surface, and the other an organically modified surface. The CSPEs were prepared by adding ionic liquids (IL) to the PEGA and the ratios between PEGA and IL were 7 : 3 and 5 : 5, respectively. The functionalized silica was synthesized by the sol-gel method under acidic conditions using methacryloxypropyl trimethoxysilane (MAPTMS), whereas the effects of silica filler on the electrochemical and thermal properties of CSPEs were investigated using electrochemical impedance spectroscopy, cyclic voltammetry, and differential scanning calorimetry. The ionic conductivity of CSPEs based on PEGA/[OTF]_$SiO_2$ at various concentrations of [EMIm][OTF] was $5.7\times10^{-4}$ and $4.8\times10^{-4}$ S/cm, and their specific capacitance was 10.0 and 9.5 F/g, respectively. With the addition of silica filler, the ionic conductivity and specific capacitance of the synthesized CSPEs were lower than those of the neat CSPEs.

Keywords: Poly(Ethylene Glycol) Monomethyl Ether Acrylate (PEGA), Composite Solid Polymer Electrolytes, Supercapacitors, Silica Filler, Structural Supercapacitors

## INTRODUCTION

Supercapacitors are energy storage devices with high mechanical robustness, high power density, fast charging/discharging rate, high cycle stability, and safety [1-3]. They can be used in pulse power supplies, hybrid electric vehicles, medical equipment, and memory protection devices [4-7]. Supercapacitors can also store energy by forming an electrical double layer (EDL) at the interface between the electrolyte and activated carbon electrode [8]. Although polymer electrolytes have better stability without leakage and can be made into ultra-thin forms, they are limited by the high interfacial resistance between the electrode and electrolyte, and low ionic conductivity [9]. Therefore, several studies have attempted to enhance the amorphous part of the electrolyte [10]. Efforts made to achieve high amorphous content of the polymer electrolyte have focused on the use of branched and/or cross-linked polymers rather than linear ones and the addition of liquid plasticizer and/or inorganic filler.

Composite solid polymer electrolytes (CSPEs) containing mesoporous nanoparticles have better mechanical stability and excellent interfacial property between the electrode and electrolyte [11,12].

In this study, we prepared a structural supercapacitor using CSPE and an epoxy prepreg/carbon fiber fabric, which was used as the packing material. CSPE was synthesized by hardening the mixture of the PEGA oligomer, silica filler, ionic liquids, and curing agent used for structural supercapacitor applications. The purpose of this study was to elucidate the effect of the content of this mixture on the electrochemical properties of CSPE with polymer electrolytes. The structural and electrochemical performance of the samples was characterized.

## EXPERIMENTAL

### 1. Materials

Poly(ethylene glycol) monomethyl ether acrylate (PEGA, Mn 480) and cumene hydroperoxide (CHP; 80%) were purchased from Aldrich. 1-Ethyl-3-methylimidazolium trifluoromethanesulfonate [[C-tri Co.; EMIm][OTF]) was used without further purification. Silica [A200, Degussa Co.] was dried under vacuum conditions at 70 °C for 24 h. Methacryloxypropyltrimethoxy silane (MAPTMS, Jusei Chemical Co.), toluene, acetic acid, and ethanol were used as obtained.

### 2. Preparation of MAPTMS-modified Silica Nanoparticles ($mSiO_2$)

The silica nanoparticle surface was modified by the sol-gel method under acidic conditions using methacryloxypropyl trimethoxysilane (MAPTMS) [13]. The three reaction mechanisms between MAPTMA and silica nanoparticles are depicted in Scheme 1. The silica nanoparticles (10.00 g) in toluene (250 ml) were added to a 500-ml four-necked flask fitted with a mechanical stirrer, thermocouple, dropping funnel, and condenser at the reflux temperature under nitrogen atmosphere, whereas MAPTMS was added dropwise. Different concentrations of MAPTMS (5, 10, and 20 g based on 10 g of silica) were added to ethanol (25 ml) at adjusted pH values. The pH of the solution was adjusted to 3-4 using an acetic acid solution. After the addition, the mixture was heated and stirred for

†To whom correspondence should be addressed.
E-mail: kkim@kitech.re.kr
‡These authors contributed equally.

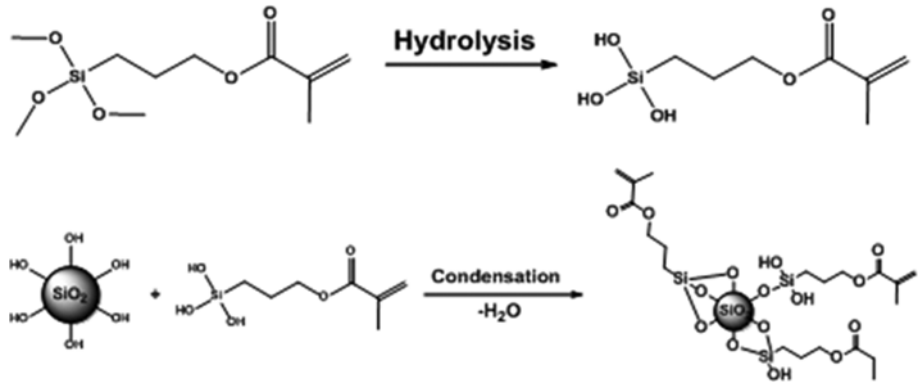


**Scheme 1. Schematic illustration of synthesis of modified silica nanoparticles.**

**Table 1. The recipe for each modified silica**

| Sample | Silica (g) | MAPTMS (g) | Toluene (ml) | Ethanol (ml) |
|---|---|---|---|---|
| $mSiO_2$(0.5) | 10 | 5 | 250 | 25 |
| $mSiO_2$(1.0) | 10 | 10 | 250 | 25 |
| $mSiO_2$(2.0) | 10 | 20 | 250 | 25 |

**Table 2. The composition of PEGA /IL based composite solid polymer electrolytes**

| Symbol | PEGA | [EMIm][OTF] | Silica filler |
|---|---|---|---|
| PEGA | 10 | - | - |
| PEGA[OTF]_91 | 9 | 1 | |
| PEGA[OTF]_73 | 7 | 3 | |
| PEGA[OTF]_55 | 5 | 5 | |
| PEGA[OTF]_S0_91 | 9 | 1 | 0.1 |
| PEGA[OTF]_S0_73 | 7 | 3 | 0.1 |
| PEGA[OTF]_S0_55 | 5 | 5 | 0.1 |
| PEGA[OTF]_ S0.5_91 | 9 | 1 | 0.1 |
| PEGA[OTF]_ S0.5_73 | 7 | 3 | 0.1 |
| PEGA[OTF]_ S0.5_55 | 5 | 5 | 0.1 |
| PEGA[OTF]_ S1.0_91 | 9 | 1 | 0.1 |
| PEGA[OTF]_ S1.0_73 | 7 | 3 | 0.1 |
| PEGA[OTF]_ S1.0_55 | 5 | 5 | 0.1 |
| PEGA[OTF]_ S2.0_91 | 9 | 1 | 0.1 |
| PEGA[OTF]_ S2.0_73 | 7 | 3 | 0.1 |
| PEGA[OTF]_ S2.0_55 | 5 | 5 | 0.1 |

2 h, after which modified silica dispersion was obtained. The product was centrifuged and washed with ethanol five times, dried in a vacuum oven at 80 °C for 24 h and ground into powder. The modified silica nanoparticles were analyzed by FT-IR, where $mSiO_2$ is a silica nanoparticle with a methacryloxypropyltrimethoxy silane group on the surface. Table 1 shows the recipe and sample code for each experiment.

**3. Preparation of PEGA-based Composite Solid Polymer Electrolytes**

We prepared CSPEs using RAFT polymerization [14]. The constituents of CSPEs based on PEGA/ILs are listed in Table 2. CHP and ILs were added to the PEGA and stirred for 1 h and the solution was dropped onto a glass plate. Next, the viscous solution was heated at 80 °C for 16 h and then heated to 110 °C for 1 h. CHP was added in a resin with a 1.5-wt% quantity. The electrolyte was named as poly(PEGA/[OTF]_I_AB) electrolyte. I, A, and B represent the type of silica filler, content of PEGA, and composition of ionic liquids, respectively.

**4. Preparation of Structural Supercapacitors**

Supercapacitors were prepared by sandwiching CSPEs between activated carbon electrodes, which was then vacuum sealed with glass fiber and carbon fiber prepreg. This supercapacitor manufacturing process was introduced in an earlier work [15-18]. The glass fiber prepreg was used in short-circuit protection [19-22]. The supercapacitors were then sandwiched between peel-plies and the mold formed was sealed with a vacuum bag and butyl. The mold was moved into an oven and heated under vacuum conditions [23]. A schematic illustration of the bagged lay-up is shown in Fig. 1.

**5. Measurements**

5-1. Fourier-transform Infrared Attenuated Total Reflection (FTIR-ATR) Spectroscopy

FTIR-ATR was characterized using the Avator 360 ESP. The microscope was placed in dry nitrogen. The spectra were recorded in a spectral range from 4,000 to 525 $cm^{-1}$, 128 scans with a resolution of 4 $cm^{-1}$ and corrected to the background spectrum of air.

5-2. Thermogravimetric Analysis

Thermogravimetric analysis (TGA) involved using a TA Instrument Q500 TGA in the temperature range from 30 to 600 °C at a heating rate of 10 °C $min^{-1}$ in an inert atmosphere with a sample weight of about 8-10 mg.

5-3. Differential Scanning Calorimetry (DSC)

Measurements were performed using a TA Instruments Q100 DSC equipped with an aluminum pan operating in an inert atmosphere. The DSC was calibrated using indium. Characterizations were carried out between −80 and 80 °C at a heating rate of 10 °C $min^{-1}$. The glass transition temperature ($T_g$) was reported as the midpoint temperature of the baseline shift measured during the transition, and the melting temperature was determined from the peak of the endotherm. The sample weight was 8-10 mg.

5-4. Electrochemical Impedance Spectroscopy (EIS)

EIS was performed to investigate the ionic conductivity of the electrolyte using an impedance analyzer, the ZIVE SP2 (WonA

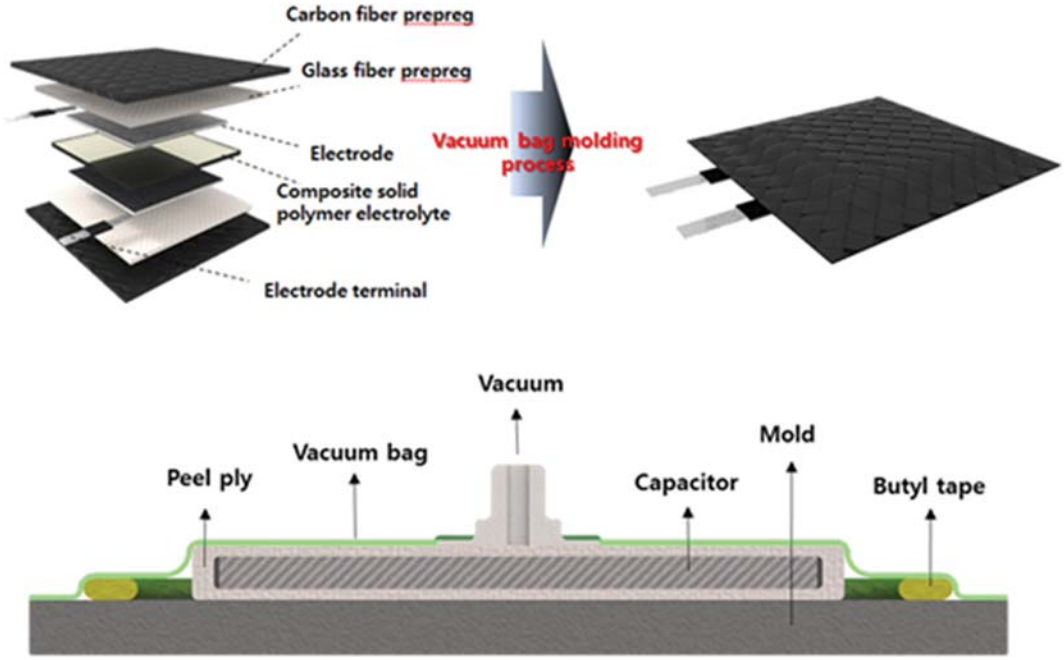


**Fig. 1. Schematic illustrating manufacturing process of structural supercapacitors.**

tech.) model. Measurements were made over frequencies ranging from 1 Hz to 1 MHz at room temperature and with an amplitude of 10 mV. Conductivity ($\sigma$) was calculated using the following equation:

$$\sigma = \frac{1}{R} \times \frac{l}{A} \quad (1)$$

where A is the area of the film [$cm^2$] and $l$ is the thickness [cm].

5-5. Cyclic Voltammetry (CV)

CV was conducted using the ZIVE SP2. A scan rate of 10 mV $s^{-1}$ was used over the range from 0 to 3 V. The specific capacitance of cells was calculated as follows:

$$C = \frac{\int I\, dV}{\nu m V} \quad (2)$$

where C, V, I, and m are the specific capacitance of the cell [F $g^{-1}$], voltage range [V], scan rate [mV $s^{-1}$], current density [A $cm^{-2}$], and mass of the active material of the electrode [g], respectively.

**6. Galvanostatic Charge-discharge Test**

Galvanostatic charge-discharge tests of the supercapacitors were performed using a WBCS 3000 (WonA tech, Korea). The galvanostatic charge-discharge test of the supercapacitors was conducted at voltage ranging from 0 to 3 V at various current densities (0.25 mA $cm^{-2}$ and 0.5 mA $cm^{-2}$).

The discharging capacitance was calculated using the following equation:

$$C = \frac{\Delta t \cdot I}{m \cdot \Delta V} \quad (3)$$

where C, m, ΔV, Δt, and I are the specific capacitance of the cell [F $g^{-1}$], total mass of the active material for the electrode [g], voltage range [V], discharge time [s], and discharging current [A], respectively.

**7. Mechanical Properties Analysis**

Tensile properties were determined in a universal testing machine. The specimen was mashed at the end of the samples. The grip distance of the end points was 40 mm and crosshead speed was 10 mm $min^{-1}$. The force was detected throughout the test continuously. The measured data was calculated with thickness and distance of the samples, expressed in equation as:

$$F_{cal} = \frac{F}{td} \quad (4)$$

where F is the average force, d is distance of the ends and t is thickness of the samples.

## RESULTS AND DISCUSSION

**1. Synthesis of Modified Silica**

MAPTMS grafted onto silica nanoparticles was investigated by FT-IR and TGA. Silica nanoparticles with methacryloxypropyltrimethoxy silane groups on the surface were investigated using FTIR-ATR. The spectra obtained from silica nanoparticles ($SiO_2$) and modified silica ($mSiO_2$) are shown in Fig. 2. The peaks in the range 1,000-1,100 $cm^{-1}$ and around 815 $cm^{-1}$ represented in Fig. 2 correspond to Si-O-Si symmetric and asymmetric stretching vibration modes in silica nanoparticles. In the FTIR-ATR spectra, the broad peak at 3,300-3,400 $cm^{-1}$ due to Si-OH stretching bond decreased in intensity and a sharp peak at 1,720 $cm^{-1}$, and those at 1,640 and 935 $cm^{-1}$, corresponding to the C=O and C=C bonds, respectively, of the methacrylate group appeared. In addition, the peaks in the range 1,000-1,100 $cm^{-1}$ and around 815 $cm^{-1}$ (Fig. 2) correspond to Si-O-Si symmetric and asymmetric stretching vibration modes, respectively, in the silica nanoparticles, indicating that MAPTMS was grafted onto the surface of silica nanoparticles. The peak in the

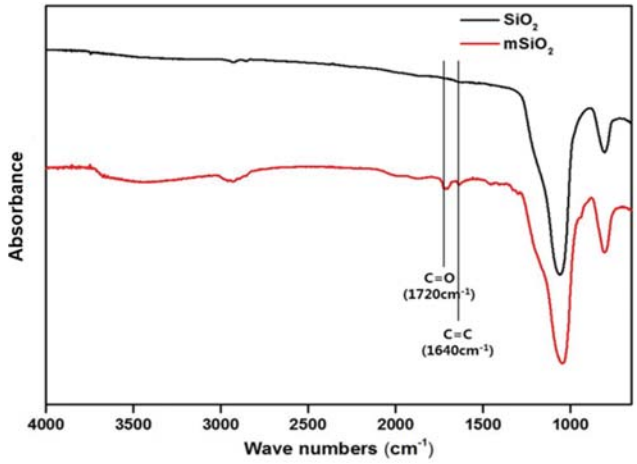


**Fig. 2. FT-IR spectra of silica and modified silica.**

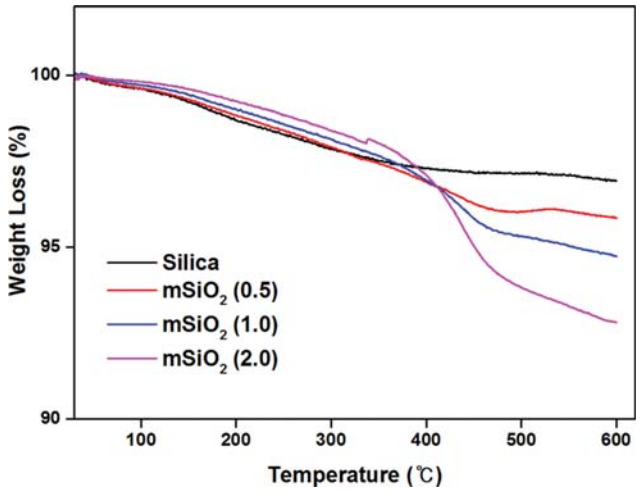


**Fig. 3. TGA curves of MAPTMS-modified silica nanoparticles.**

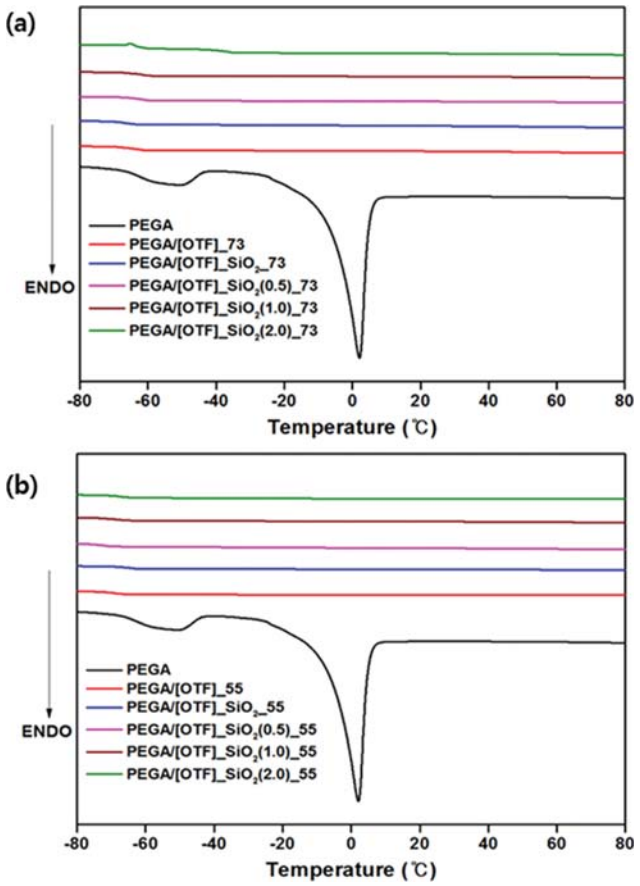


**Fig. 4. DSC thermogram of PEGA/[OTF]-based composite solid polymer electrolytes.**

range 1,000-1,100 $cm^{-1}$ due to the Si-O-C antisymmetric stretching mode shifted to a lower frequency. Moreover, there was no big difference in FT-IR spectra according to modifying degree. That may because of the small differences of modifying degree within $mSiO_2$(0.5) to $mSiO_2$(2.0).

A successful modification reaction was also confirmed from the weight loss data obtained by TGA between silica nanoparticles and MAPTMS-modified silica nanoparticles. TGA was conducted on the modified silica nanoparticles in an inert atmosphere to characterize thermal stability. Fig. 3 shows the TGA curves for silica nanoparticles and MAPTMS-modified silica nanoparticles. For silica nanoparticles, the weight loss from 30 to 350 °C was 2.9 wt% due to the desorption of physically adsorbed water and water in the Si-OH condensation step. For MAPTMS-modified silica nanoparticles, the decomposition temperature was 427 °C. The weight loss of MAPTMS-modified silica nanoparticles for different concentrations of MAPTMS was 4.2, 5.5, and 7.6%, respectively. For MAPTMS-modified silica nanoparticles, the weight loss for different concentrations of MAPTMS from 30 to 350 °C was 2.5, 2.3, and 1.9%, respectively, because many of the Si-OH groups were used in the silylation reaction. The grafting efficiency of MAPTMS on silica nanoparticles increased with MAPTMS concentration.

**2. Preparation of Composite Solid Polymer Electrolyte**

DSC was used to investigate the morphology of the organic polymer phase in the composite solid polymer electrolyte and also to determine the nature and degree of PEGA-[OTF] and PEGA-silica filler interaction. Fig. 4 shows the DSC thermogram curves for the composite solid polymer electrolyte using silica nanoparticles and MAPTMS-modified silica nanoparticles. The glass transition temparature ($T_g$) and melting temperature ($T_m$) were investigated using DSC (Table 3). Poly(ethylene glycol) monomethylether acrylate (PEGA) exhibited $T_g$ and $T_m$ at −61 °C and 5 °C, respectively. As [EMIm] [OTF] was added to solid polymer electrolytes, melting temperature disappeared owing to a decrease in crystallinity. The value of $T_g$ for PEGA/[OTF]-based polymer electrolytes with different concentrations of [EMIm][OTF] was −64 and −69 °C, respectively. As the ionic liquid concentration increased, $T_g$ decreased. DSC results indicate that the glass transition temperature of PEGA generally shifted towards a low temperature with the addition of [EMIm] [OTF] and silica filler because the PEGA-[OTF] and PEGA-silica filler interactions for composite solid polymer electrolytes were decreased.

The mechanical property of CSPEs was studied, which is presented in Fig. S1. The mechanical property of full cell was in pro-

**Table 3. The thermal properties of PEGA/[OTF] based composite solid polymer electrolytes**

| Sample | $T_g$ (°C) | $T_m$ (°C) |
|---|---|---|
| PEGA | −61 | 5 |
| PEGA[OTF]_73 | −64 | - |
| PEGA[OTF]_55 | −69 | - |
| PEGA[OTF]_$SiO_2$_73 | −66 | - |
| PEGA[OTF]_$SiO_2$_55 | −65 | - |
| PEGA[OTF]_$mSiO_2$ (0.5)_73 | −62 | - |
| PEGA[OTF]_$mSiO_2$ (0.5)_55 | −73 | - |
| PEGA[OTF]_$mSiO_2$ (1.0)_73 | −62 | - |
| PEGA[OTF]_$mSiO_2$ (1.0)_55 | −68 | - |
| PEGA[OTF]_$mSiO_2$ (2.0)_73 | −61 | - |
| PEGA[OTF]_$mSiO_2$ (2.0)_55 | −68 | - |

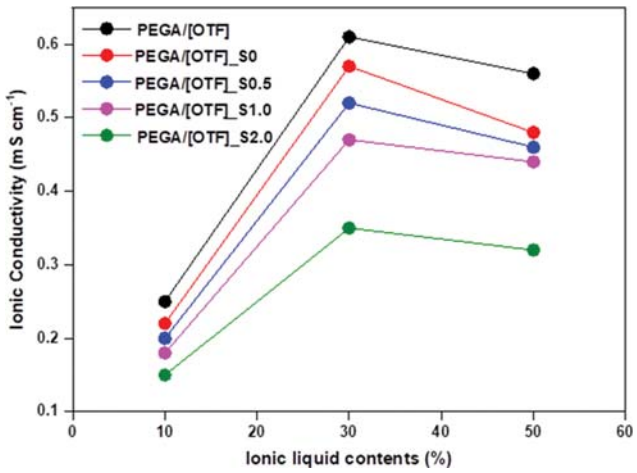


**Fig. 5. Ionic conductivity of CSPEs with different content of [EMIm][OTF].**

portion to carbon fiber composite, not to the composition of gel electrolytes. Therefore, we tested the mechanical property of one of full cells. Tensile strength and tensile modulus of full cell were 116.9 MPa and 9.05 GPa. Fig. 5 shows ionic conductivity calculated using EIS data. The ionic conductivity of CSPEs based on PEGA/[OTF] was 0.25 and 0.61 and 0.56 mS $cm^{-1}$, respectively. The ionic conductivity values of the CSPEs depend on the composition of the completing effects [24]. As the concentration of IL increased to 30%, ionic conductivity was enhanced owing to the composition of the ion transference number, but ionic conductivity was decreased in case of 50% of IL. In contrast, the ionic conductivity of the samples with silica filler decreased due to the ion-dipolar moment and ion pair [24]. The ionic conductivity of PEGA/[OTF]_$SiO_2$-based CSPEs was 0.22, 0.57 and 0.48 mS $cm^{-1}$, respectively. The ionic conductivity of PEGA/[OTF]_$mSiO_2$_91-based CSPEs with a grafting efficiency of MAPTMS on silica nanoparticles was 0.20, 0.18 and 0.15 mS $cm^{-1}$, respectively. The ionic conductivity of PEGA/[OTF]_$mSiO_2$_73-based CSPEs with a grafting efficiency of MAPTMS on silica nanoparticles was 0.52, 0.47 and 0.35 mS $cm^{-1}$, respectively. The ionic conductivity of PEGA/[OTF]_$mSiO_2$_55-based CSPEs with a grafting efficiency of MAPTMS on silica nanoparticles was

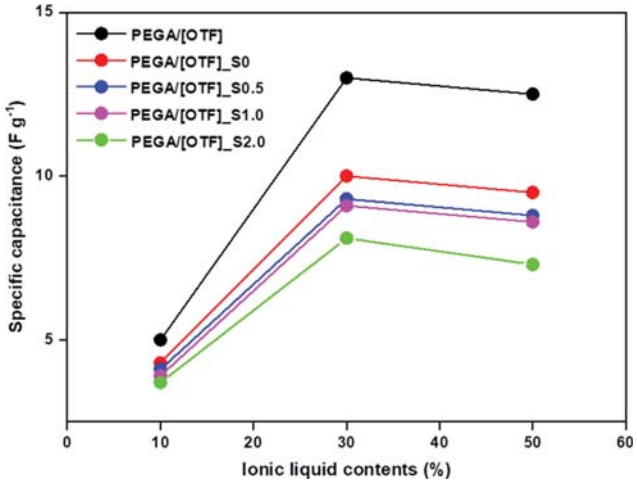


**Fig. 6. Specific capacitance of CSPEs using cyclic voltammetry.**

0.46, 0.44 and 0.32 mS $cm^{-1}$, respectively. The ionic conductivity of CSPEs decreased as silica filler was added. Owing to the OH group content of silica surface, the ionic conductivity of CSPEs with $SiO_2$ was higher than that of CSPEs with $mSiO_2$.

Cyclic voltammetry was conducted at room temperature over voltages ranging from 0 to 3 V at a scan rate of 10 mV $s^{-1}$. The specific capacitance of the supercapacitor calculated from the CV curves (Fig. S1) is shown in Fig. 6. The composition of PEGA and ionic liquids was 9 : 1 7 : 3 and 5 : 5, respectively. The specific capacitance of CSPEs based on PEGA/[OTF] with various concentrations of [EMIm][OTF] was 5, 13.0 and 12.5 F $g^{-1}$, respectively. As the concentration of IL increased to 30%, specific capacitance was enhanced, but the capacitance was decreased in case of 50% of IL. The specific capacitance of PEGA/[OTF]_$SiO_2$-based CSPEs with various concentrations of [EMIm][OTF] was 4.3, 10.0 and 9.5 F $g^{-1}$, respectively. The specific capacitance of the PEGA/[OTF]_$mSiO_2$_91 based CSPEs with a grafting efficiency of MAPTMS on silica nanoparticles was 4.1, 3.9and 3.7 F $g^{-1}$, respectively. The specific capacitance of the PEGA/[OTF]_$mSiO_2$_73 based CSPEs with a grafting efficiency of MAPTMS on silica nanoparticles was 9.3, 9.1, and 8.1 F $g^{-1}$, respectively. The specific capacitance of the PEGA/[OTF]_$mSiO_2$_55-based CSPEs with a grafting efficiency of MAPTMS on silica nanoparticles was 8.8, 8.6, and 7.3, respectively. The specific capacitance of CSPEs with $SiO_2$ was higher than that of CSPEs with $mSiO_2$. As the grafting ratio of MAPTMS on silica nanoparticles increased, the specific capacitance of CSPEs decreased.

The structural supercapacitor was tested using galvanostatic charging-discharging at current density of 0.25 and 0.5 mA $cm^{-2}$. Figs. 7(a) and (b) show the galvanostatic charging-discharging curves of the structural capacitor with PEGA/[OTF] at various current densities. Figs. 7(c) and (d) show the galvanostatic charging-discharging curves of the supercapacitors with PEGA/[OTF]_55_S2.0 at various current densities. The specific capacitance of the supercapacitors using the galvanostatic charging-discharging test is shown in Table S2. In case of PEGA/[OTF], the specific capacitance at 0.25 mA $cm^{-2}$ was 68 and 55 F $g^{-1}$ for PEGA/[OTF]_73 and PEGA/[OTF]_55, and the specific capacitance at 0.5 mA $cm^{-2}$ was 30 and 28 F $g^{-1}$, respectively. In the PEGA/[OTF]_S2.0 case, the specific

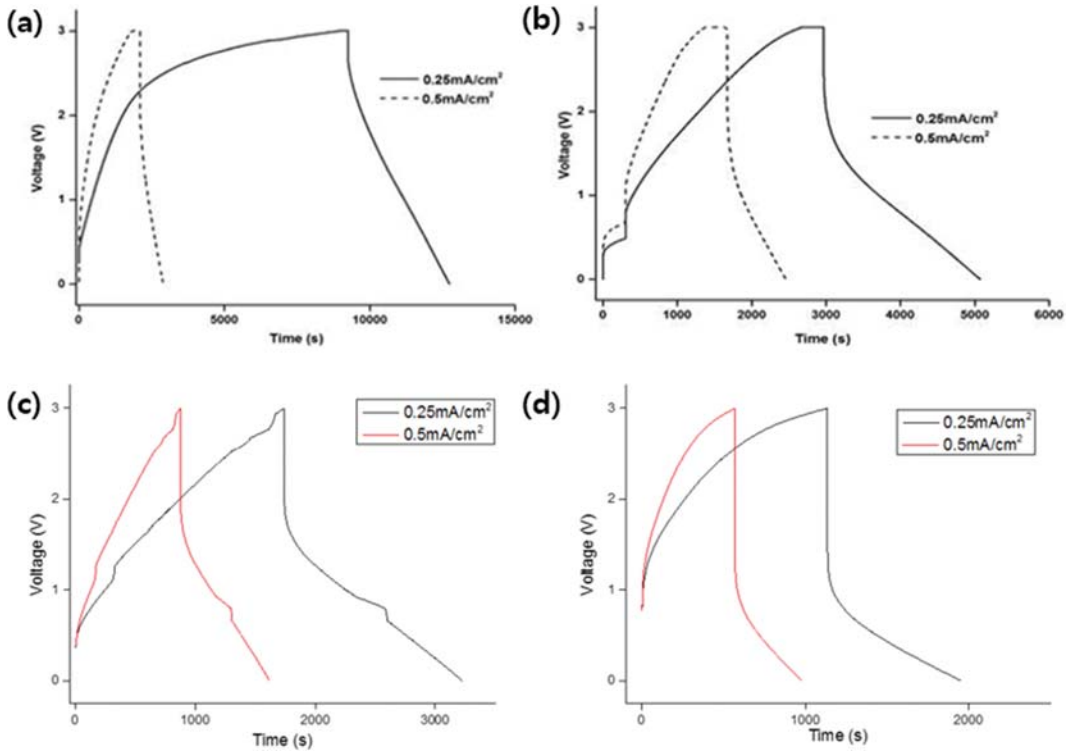


**Fig. 7. Galvanostatic charging/discharging curves of (a) PEGA/[OTF]_73, (b) PEGA/[OTF]_55, (c) PEGA/[OTF]_73_S2.0 and (d) PEGA/[OTF]_55_S2.0 at the different current density.**

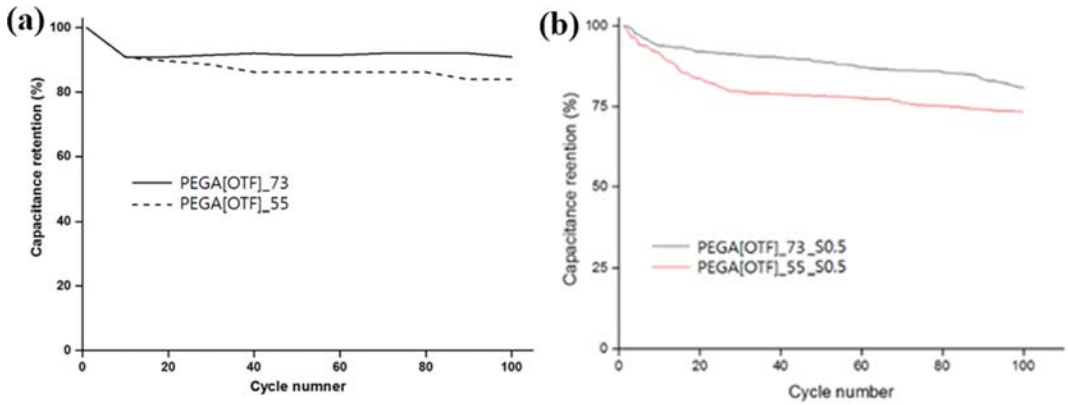


**Fig. 8. Cycling performance of PEGA with different concentrations of [EMIm][OTF] and modified silica over 100 cycles.**

capacitance at 0.25 mA $cm^{-2}$ was 45 and 23 F $g^{-1}$ and the specific capacitance at 0.5 mA $cm^{-2}$ was 30 and 11 F $g^{-1}$ for PEGA/[OTF]_73_S2.0 and PEGA/[OTF]_55_S2.0, respectively. As the current density increased, specific capacitance decreased. The relative specific capacitance of CSPEs tended to decrease with the addition of silica. As silica filler was added, the specific capacitance of the CSPEs decreased. Because of the OH-group content of the silica surface, the specific capacitance of CSPEs with $SiO_2$ was higher than that of CSPEs with $mSiO_2$. Ohmic drops occurred in all samples due to the contact resistance of the electrode and electrolyte and the internal resistance [25]. As the IL content increased, specific capacitance increased.

The cycle stability of structural capacitors is an important characteristic for practical applications. Cycling tests were performed using the CV method and capacitance retention (CR) was calculated using the following equation:

$$CR = \frac{C_n}{C_0} \times 100 \quad (5)$$

where $C_n$ is the discharging capacitance at each cycle, and $C_0$ is the discharging capacitance in the first cycle. Figs. 8(a) and (b) show the CR of a capacitor of the PEGA/[OTF] series. After 100 cycles, the CR of PEGA/[OTF]_73 and PEGA/[OTF]_55 was approximately 91% and 84%, respectively. In the PEGA/[OTF]_73_S0.5 and PEGA/[OTF]_55_S0.5 cases, the capacitance retention was 81% and 76%, respectively. The PEGA/[OTF]_73 electrolyte exhib-

ited better stability than that of the PEGA/[OTF]_55 electrolyte. The PEGA_73 electrolyte process demonstrated an excellent lifetime during repetitive charge-discharge cycling. However, these results appear to be because the number of ions in the PEGA/[OTF]_55 sample is greater than that in the PEGA/[OTF]_73 sample. Therefore, the CR values further reduced as the interaction between the electrode and the electrolyte became more active.

## CONCLUSIONS

We prepared CSPEs using [EMIm][OTF] as the IL, PEGA as the oligomer, and silica filler, at two different ratios between PEGA and ionic liquid (7 : 3 and 5 : 5). In the FT-IR spectrum of modified $SiO_2$, the mean peaks were as follows: C=O stretching (carbonyl peak) at 1,720 $cm^{-1}$ and C=C peak at 1,640 $cm^{-1}$ and 935 $cm^{-1}$. In the TGA, the decomposition temperature of modified silica was 427 °C. The modification rate of silica was 4.2%, 5.5%, and 7.6%, respectively. The DSC thermograms showed that PEGA had a glass transition temperature of −61 °C and a melting temperature of 5 °C. The $T_g$ of the polymer electrolyte was lower than that of PEGA. The $T_m$ of CSPE disappeared due to the addition of ionic liquid, while the crystalline structure disappeared. The electrochemical performance of CSPEs for structural supercapacitors was studied using EIS and cyclic voltammetry. The ionic conductivity of PEGA/[OTF]-based CSPEs was 0.61 mS $cm^{-1}$, in case of 30% of ionic liquid. The ionic conductivity of PEGA/[OTF]_$SiO_2$-based CSPEs was 0.57 mS $cm^{-1}$, in case of 30% of ionic liquid. With the addition of silica filler, the ionic conductivity of synthesized CSPEs was lower than that of the neat CSPEs. The specific capacitance of PEGA/[OTF] with 30% of [EMIm][OTF] was 11.5 F $g^{-1}$ and of the PEGA/[OTF]_$SiO_2$-based CSPEs was 10.0 F $g^{-1}$, respectively. Under the references, mesoporous silica can increase mechanical properties of solid electrolytes. We confirmed the silica filler decreased the electrochemical performance of the electrolytes. Finally, we concluded that silica filler in the EMIM : OTF based electrolyte has a trade-off between mechanical and electrochemical performance. Moreover, we confirmed 30% of ionic liquid content was best in case of PEGA/[OTF] polymer electrolyte. Additionally, we thought that our devices had poor electrochemical performance because of the ionic conductivity of the electrolyte and contact resistance of electrode/electrolyte interface. So, we will try to increase the electrochemical performance through additional experiments about the content of electrolytes or additives for electrolytes.

## ACKNOWLEDGEMENTS

This study was conducted with the support of the Korea Institute of Industrial Technology as "Development of Smart Energy Storage Structural Composites" (KITECH-EO-170052), and supported by the Technology Innovation Program (20007161, Localization of Source Materials and Development of Application Technology for High Modulus PAN based Carbon Fibers) funded by the Ministry of Trade, Industry & Energy (MOTIE, Korea).

## SUPPORTING INFORMATION

Additional information as noted in the text. This information is available via the Internet at http://www.springer.com/chemistry/journal/11814.

## REFERENCES

1. P. Simon and Y.gogotsi, *Nat. Mater.*, **19**, 1151 (2020)
2. J. P. Cheng, W. D. Wang, X. C. Wang and F. Liu, *Chem. Eng. J.*, **393**, 124747 (2020).
3. B. E. Conway, *Electrochemical supercapacitors*, Springer Science & Business Media, New York (1999)
4. W. Raza, F. Ali, N. Raza, Y. Luo, K. H. Kim, J. Yang, S. Kumar, A. Mehmood and E. E. Kwon, *Nano Energy*, **52**, 441 (2018).
5. J. Chmiola, G. Yushin, Y. Gogotsi, C. Portet, P. Simon and P. L. Taberna, *Science*, **313**, 1760 (2006).
6. A. Borenstein, O. Hanna, R. Attias, S. Luski, T. Brousse and D. Aurbach, *J. Mater. Chem. A*, **5**, 12653 (2017).
7. T. Liu, F. Zhang, Y. Song and Y. Li, *J. Mater. Chem. A*, **5**, 17705 (2017).
8. J. Xie, P. Yang, Y. Wang, T. Qi, Y. Lei and C. M. Li, *J. Power Sources*, **401**, 213 (2018).
9. L. Long, S. Wang, M. Xiao and Y. Meng, *J. Mater. Chem. A*, **4**, 10038 (2016).
10. J. Zhang, J. Yang, T. Dong, M. Zhang, J. Chai, S. Dong, T. Wu, X. Zhou and G. Cui, *Small*, **14**, 1800821 (2018).
11. W. Wang and P. Alexandridis, *Polymers (Basel)*, **8**, 387 (2016).
12. D. Lin, W. Liu, Y. Liu, H. R. Lee, P. C. Hsu, K. Liu and Y. Cui, *Nano Lett.*, **16**, 459 (2016).
13. J. Zhang, Z. Guo, X. Zhi and H. Tang, *Colloids Surf. A Physicochem. Eng. Asp.*, **418**, 174 (2013).
14. A. R. Mazo, T. N. Tran, W. Zhang, Y. Meng, A. Reyhani, S. Pascual, L. Fontaine, G. G. Qiao and S. Pioge, *Polym. Chem.*, **11**, 5238 (2020).
15. J. Thomas, S. Qidwai, W. Pogue and G. Pham, *J. Compos. Mater.*, **47**, 5 (2013).
16. Y. Lin and H. A. Sodano, *J. Appl. Phys.*, **106**, 114108 (2009).
17. X. Luo and D. D. L. Chung, *Sci. Technol.*, **61**, 885 (2001).
18. B. S. Cho, J. Choi and K. Y. Kim, *Fibers Polym.*, **18**, 1452 (2017).
19. A. Javaid, K. K. C. Ho, A. Bismarck, M. S. P. Shaffer, J. H. G. Steinke and E. S. Greenhalgh, *J. Compos. Mater.*, **48**, 1409 (2014).
20. H. Qian, A. R. Kucernak, E. S. Greenhalgh, A. Bismarck and M. S. P. Shaffer, *ACS Appl. Mater. Interfaces*, **5**, 6113 (2013).
21. T. Carlson, D. Ordéus, M. Wysocki and L. E. Asp, *Compos. Sci. Technol.*, **70**, 1135 (2010).
22. T. Carlson, D. Ordéus, M. Wysocki and L. E. Asp, *Plast. Rubber Compos.*, **40**, 311 (2011).
23. T. Carlson and L. E. Asp, *Compos. Part B Eng.*, **49**, 16 (2013).
24. Y. Wang, Z. Shi, Y. Huang, Y. Ma, C. Wang, M. Chen and Y. Chen, *J. Phys. Chem. C*, **113**, 13103 (2009).
25. K. H. An, W. S. Kim, Y. S. Park, J. M. Moon, D. J. Bae, S. C. Lim, Y. S. Lee and Y. H. Lee, *Adv. Functional Mater.*, **11**, 387 (2001).

# Supporting Information

# Composite solid polymer electrolyte with silica filler for structural supercapacitor applications

**Minsik Hwang[‡], Ji San Jeong[‡], Jae-Chul Lee, Seongil Yu, Hyun Seok Jung, Bong-Sang Cho, and Ki-Young Kim[†]**

Human Convergence Technology R&D Department, Research Institute of Convergence Technology, Korea Institute of Industrial Technology (KITECH), Gyeonggi-do 15588, Korea
(*Received 19 May 2020 • Revised 24 September 2020 • Accepted 14 October 2020*)

**Table S1. Mechanical properties of structural supercapacitor**

| Sample | Tensile strength (MPa) | Tensile modulus (GPa) |
|---|---|---|
| PEGA[OTF]_m$SiO_2$ (1.0)_73 | 116.90±12.04 | 9.05±0.80 |

**Table S2. Specific capacitance of the CSPEs**

| Sample | Current Density (F $g^{-1}$) | |
|---|---|---|
| | 0.25 mA $cm^{-2}$ | 0.5 mA $cm^{-2}$ |
| PEGA[OTF]_73 | 68 | 30 |
| PEGA[OTF]_55 | 55 | 28 |
| PEGA[OTF]_73_S2.0 | 45 | 23 |
| PEGA[OTF]_55_S2.0 | 30 | 11 |

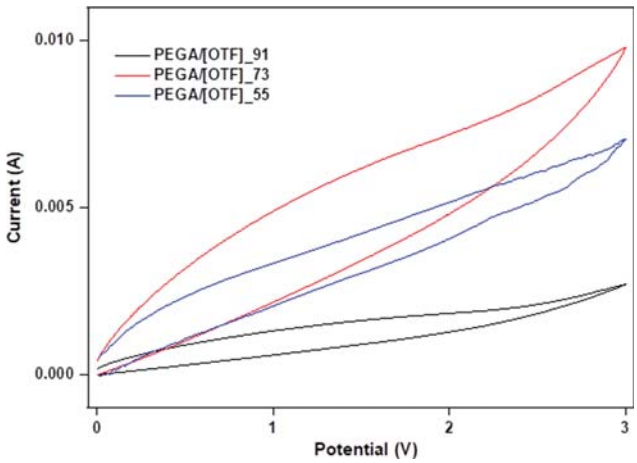


**Fig. S1. CV curves of PEGA/[OTF].**